# Spontaneous Phase Transformation and Exfoliation of Rectangular Single-Crystal Zinc Hydroxy Dodecylsulfate Nanomembranes

**Fei Wang,[†,‡] Joseph E. Jakes,[§] Dalong Geng,[†] and Xudong Wang[†,*]**

[†]Department of Materials Science and Engineering, [‡]Department of Chemistry, University of Wisconsin—Madison, Madison, Wisconsin 53706, United States, and [§]Forest Biopolymer Science and Engineering, USDA Forest Service, Forest Products Laboratory, Madison, Wisconsin 53726, United States

**ABSTRACT**

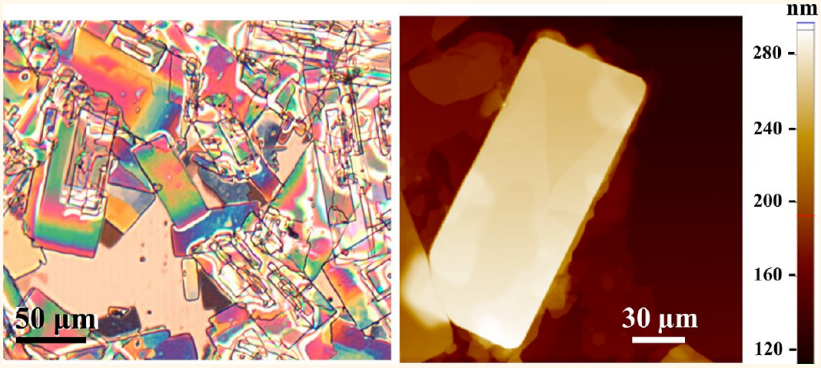


Free-standing two-dimensional (2D) nanostructures, exemplified by graphene and semiconductor nanomembranes, exhibit exotic electrical and mechanical properties and have great potential in electronic applications where devices need to be flexible or conformal to nonplanar surfaces. Based on our previous development of a substrate-free synthesis of large-area, free-standing zinc hydroxy dodecylsulfate (ZHDS) hexagonal nanomembranes, herein, we report a spontaneous phase transformation of ZHDS nanomembranes under extended reaction time. The hexagonal ZHDS sheets transformed into rectangular single crystal nanomembranes with sizes of hundreds of micrometers. They contain long-range-ordered zinc vacancies that can be fitted into an orthorhombic superlattice. A surplus of dodecylsulfate ions and a deficit of $Zn^{2+}$ diffusion near the water surface are believed to be the factors that drive the phase transformation. The phase transformation starts with the formation of zinc vacancies at the topmost layer of the hexagonal hillock, and propagates along the spiral growth path of the initial hexagonal sheets, which bears a great resemblance to the classic "periodic slip process". Mechanical property characterization of ZHDS nanomembranes by nanoindentation shows they behave much like structural polymers mechanically due to the incorporation of surfactant molecules. We also developed a one-step exfoliation and dehydration method that converts ZHDS nanomembranes to ZnO nanosheets using *n*-butylamine. This work provides a further understanding of the growth and stability of ZnO-based nanomembranes, as well as advisory insight for the further development on solution-based synthesis of free-standing, single-crystalline 2D nanostructures.

**KEYWORDS:** free-standing two-dimensional nanostructure · phase transformation · nanomembranes · exfoliation · nanoindentation · screw dislocations

Free-standing two-dimensional (2D) nanostructures, exemplified by graphene and semiconductor nanomembranes, represent one of the pivotal areas that are leading the advances in nanomaterials and nanotechnologies.[1−3] The exotic electrical and mechanical properties rising from their 2D geometry have enabled vast applications in important fields such as transistors, optoelectronics and energy harvesting devices.[4−10] While the quantum effects and size-dependent properties of 0D quantum dots and 1D nanowires/nanotubes are also exhilarating, researchers often find it difficult in leveraging the properties from individual building blocks due to myriads of challenges in the assembly and fabrication processes. In contrast, 2D structures are very

* Address correspondence to xudong@engr.wisc.edu.

Received for review April 7, 2013 and accepted June 3, 2013.

**Published online June 03, 2013**
10.1021/nn4017108

fabrication-friendly as they enjoy the mature fabrication technologies that have existed in industry for decades. Free-standing 2D nanostructures naturally inherit these advantages, but also feature in their capability of being transferred onto arbitrary substrates, and in particular, flexible transparent substrates which are otherwise incompatible with high-temperature epitaxial techniques. Therefore, applications such as flexible transparent electronics and conformal medical devices could be unlocked.[11−13]

Means of producing free-standing 2D nanostructures include selective etching of sacrificial layers as in the cases of silicon and gallium arsenide nanomembranes,[14−16] and exfoliation of naturally layered crystals as in the cases of graphene and $MoS_2$. Direct syntheses of nanosheets are only sporadical.[17−19] Nonetheless, new methods with low-cost and simple fabrication procedures need to be developed to obtain free-standing 2D nanostructures of other functional materials in order to meet the requirements of broader applications. We recently reported a surfactant-directed surface assembly approach to producing large-area zinc hydroxy dodecylsurfate (ZHDS) nanomembranes at the water−air interface and the nanomembranes could cover the entire water surface of the reaction container.[20] Unlike the conventional use of surfactants for tuning the morphology of crystal by the consensus selective surface adsorption mechanism,[21−24] we chose a materials system (zinc hydroxy sulfate) where the surfactant molecules would participate in the crystallization so that we could employ the surface Langmuir−Blodgett (LB) layer as a template to guide the 2D growth into large-area nanomembranes. This incorporation of surfactant molecules into the crystal lattice transcended the previous limitation that only nanometer-sized particles could be grown underneath the LB layer.[25−27] We also demonstrated its great potential in electronic applications by a proof-of-principle field-effect transistor.

The free-standing ZHDS nanomembranes consisted of single-crystalline hexagonal grains up to a few hundred-micrometer wide. We thereafter found that the hexagonal crystal grains would experience a phase transformation after extended reaction time and transform themselves from hexagonal sheets to rectangular sheets. In this paper, we report this intriguing phase transformation phenomenon, investigate the crystal structure of the rectangular ZHDS sheets, and discuss its origin and transformation mechanism. We found that the spiral growth of the initial hexagonal sheets that originated in screw dislocations provided a pathway for the phase transformation, which bore a great resemblance to the classic "periodic slip process" that explained the polymorphism of zinc sulfide (ZnS) and silicon carbide (SiC). Mechanical properties of ZHDS nanomembranes were characterized by nanoindentation experiments. Comparing to single-crystal ZnO sheets which exhibit typical ceramic behaviors, ZHDS nanomembranes were much softer and behaved similar to structural polymers, such as polycarbonate. We also present a one-step method that exfoliates ZHDS nanomembranes and dehydrates the zinc hydroxide layers simultaneously, and free-standing ZnO nanosheets were thereafter obtained. We note that by replacing the zinc ions with other metal ions or using other surfactants with functional groups, we could potentially develop a family of other metal hydroxyl surfactant compounds in the form of large-area nanomembranes. Combining this idea with our exfoliation technique, we could add a number of new materials to our portfolio of free-standing and flexible 2-D nanostructures.

## RESULTS AND DISCUSSIONS

**Morphology and Structural Characterization.** Figure 1 depicts the morphology of the rectangular ZHDS sheets after the phase transformation. Figure 1a is an optical microscopy image of the rectangular sheets on a silicon substrate. They are 50−100 $\mu$m in width and 100−300 $\mu$m in length. Some rectangular sheets have fairly flat surface. The AFM topography scan in Figure 1b shows a flat sheet with a thickness of 108 nm and topography variation is within 4 nm (Figure 1d). Most sheets exhibit obvious thickness variation. The color contrast in Figure 1a is a direct result of optical interference that manifests thickness variation. The sheets get thicker when the color goes from blue on the sides of the sheets to red near the center of the sheets. This thickness development coupled with the color gradient under the optical microscope shows a rectangular pattern and is better manifested by the AFM topography scan in Figure 1c. The sheets grow in a rectangular spiral motion and form surface hillocks with steps ranging from 11 to 120 nm (Figure 1e). This kind of surface topography was also found in the hexagonal sheets but with a hexagonal pattern. We discussed in our previously report that the hexagonal surface contours are a consequence of screw dislocation-driven growth.[28,29] We believe that the screw dislocations are retained during the formation of the rectangular sheets and they facilitate the phase transformation, which will be discussed later. Therefore, the surface contours remain on the rectangular sheets but with a rectangular pattern.

A low-magnification TEM image of the rectangular sheets is shown in Figure 2a. The contrast on the rectangular sheet comes from the local thickness variation and again indicates the dislocation steps. Figure 2b is the electron diffraction pattern taken from the sheet. This electron diffraction pattern contains bright spots that reveal a hexagonal symmetry as well as weak spots that can be fitted into an orthorhombic superlattice. We discussed in our previous report that the initial hexagonal ZHDS $(3Zn(OH)_2 \cdot Zn(DS)_2$, where

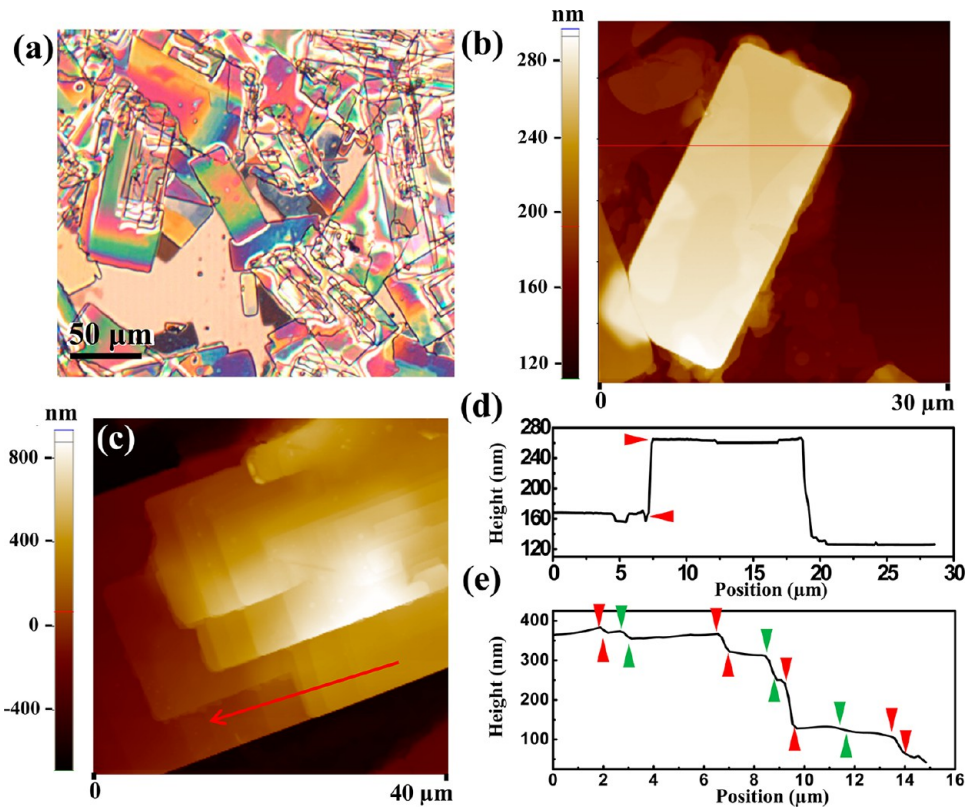


**Figure 1. Morphology of rectangular ZHDS sheets. (a) Optical microscopy image of rectangular sheets on a silicon substrate. (b) AFM topography image of an individual rectangular sheets. (c) AFM topography image of part of a rectangular sheets, revealing the surface steps that resulted from the spiral growth and spiral phase transformation. (d and e) Line profiles of the surface topography labeled by the red lines in \panels b and c, respectively. Panel d indicates a thickness of 108 nm. The dislocation steps in panel e labeled by alternating red and green cursor pairs are 11, 16, 46, 62, 121, 14, and 53 nm, respectively, from left to right.**

DS denotes dodecylsulfate) sheets are composed of pseudohexagonal zinc hydroxide layers with dodecylsulfate ions and water molecules incorporated in between the zinc hydroxide layers. The lattice spacing that corresponds to the weak diffraction spots of the rectangular sheets here equals to that of the initial hexagonal ZHDS sheet. When considering the crystal structure of the rectangular ZHDS sheets as a derivative of the hexagonal ZHDS sheets and fitting the weak diffraction spots into an orthorhombic superlattice, we find $a' = 2a$, $b' = \sqrt{3}a$, where $a'$ and $b'$ are the lattice parameters of the orthorhombic superlattice and $a$ is the zinc−zinc distance in the hexagonal ZHDS. While the charging effect of the dodecylsulfate ions made the sheets deteriorate rapidly under the electron beam and prevented us from obtaining high-resolution TEM images, this fitted epitaxial relationship led us to believe that the superlattice is composed of long-range-ordered Zn vacancies. As illustrated in Figure 2c, these Zn vacancies (white circles) take up every other Zn position in every other row in the initial hexagonal lattice. This orthorhombic Zn vacancy supperlattice has previously been observed in the nanophase on Wurtzite ZnO nanobelts.[30] In Figure 2b, the bright spots are indexed in a hexagonal system while the weak spots are indexed based on the orthorhombic superlattice.

We believe that the rectangular morphology of the ZHDS sheets results from the symmetry of the zinc vacancies (or equivalently, the remaining zinc ions). We also quantified the relative contents of zinc and sulfur by X-ray photoelectron spectroscopy (XPS). The results informed us that the relative zinc content with respect to sulfur decreased greatly after the phase transformation (Figure S1). Small-angle X-ray diffraction pattern was obtained in order to calculate the *c*-direction lattice parameter (Figure 1d). We see the (001) peak at 2.03° and higher-order diffractions at higher angles. The corresponding lattice spacing is 4.3 nm, a slight increase from that of the hexagonal sheets (2.20° and 4.0 nm). With the zinc hydroxide layers loosing half of the zinc ions, this increase indicates a more up-straight orientation of the hydrocarbon chains in $DS^-$ ions. The inset in Figure 1d is a magnified view of the X-ray diffraction pattern from 10° to 30°. There are a few very small peaks (labeled by solid square dots) that are spaced out by about 3° and are identified as high-order (001) peaks.

**Phase Transformation Process.** To investigate the *in situ* evolution of the rectangular phase from the hexagonal phase, the nanosheets formed on water surface were collected at different reaction time intervals. Figure 3a shows the initialization and development of the

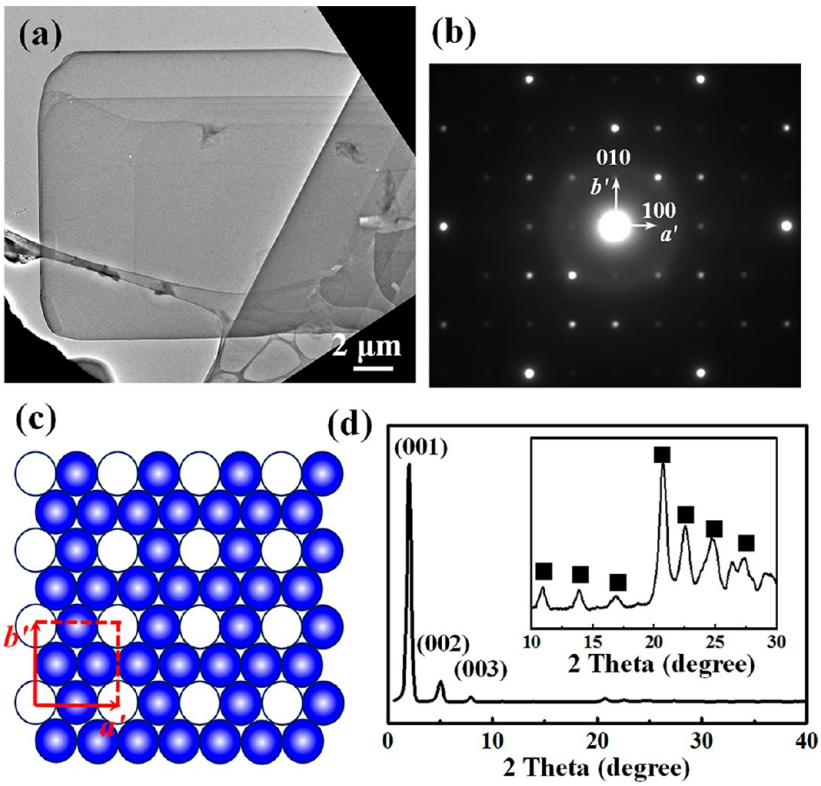


**Figure 2. Structural characterization of rectangular ZHDS sheets. (a) Low-magnification TEM image of an individual rectangular sheet. (b) Corresponding electron diffraction. (c) Schematic illustration of the zinc vacancy superlattice. The solid blue spheres represent $Zn^{2+}$ and the white circles represent zinc vacancies. The unit cell vectors of the superlattice are marked as $a'$ and $b'$. (d) X-ray diffraction pattern. The inset is an enlarged view showing the details from 10° to 30°.**

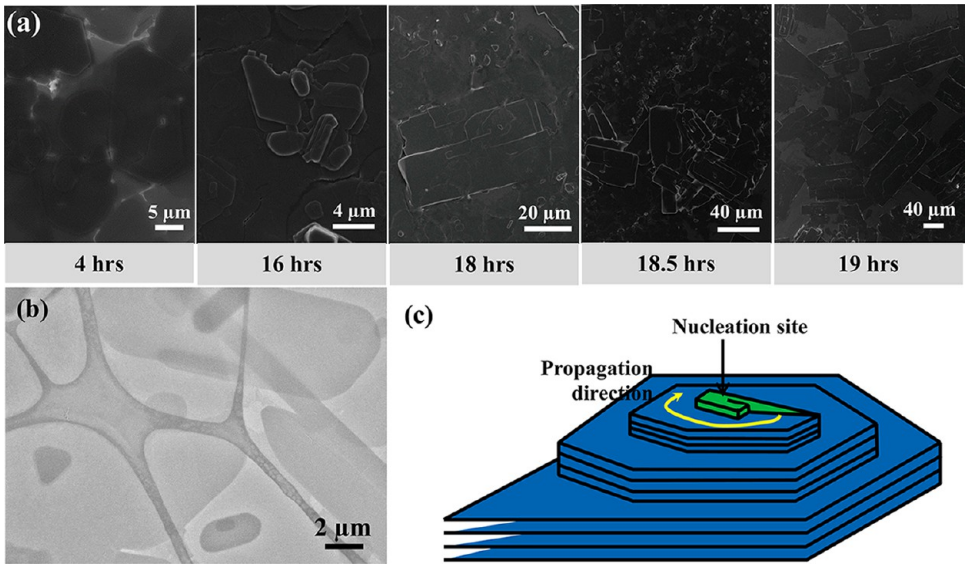


**Figure 3. Evolution of rectangular ZHDS sheets from hexagonal ZHDS sheets. (a) SEM images of ZHDS sheets collected from growth chamber at 4, 16, 18, 18.5, and 19 h, respectively. (b) TEM image of nascent rectangular ZHDS sheets on top of the hexagonal ZHDS sheets in the middle of the phase transformation. (c) Schematic illustration of the path of the phase transformation.**

rectangular phase when 25 mM zinc nitrate and HMT and 20 mM SDS were used. At 4 h, the continuous nanomembranes were comprised of hexagonal crystal sheets, entirely. After ~16 h of reaction, the orthorhombic phase in the form of rectangular sheets started to appear over the hexagonal sheets. Two hours later, a greater amount of rectangular sheets were found. They grew bigger with a few more dislocation steps while new nascent ones formed too. At 18.5 h, the trend sustained, and after 19 h, large-sized rectangular

sheets were formed at the expense of all the initial hexagonal sheets.

We note that these nascent rectangular sheets were in smaller sizes compared to the hexagonal steps at the topmost of the hillocks and stemmed at the center of the surface hillocks. The TEM image in Figure 3b corroborated this observation. This suggested that the screw dislocations which gave rise to the spiral growth of the hexagonal sheets should also play an important role in the ZHDS phase evolution. In other dislocation-rich and close-packed materials such as ZnS and SiC, the phase transformations between different polytypes are triggered by a stacking fault that changes the Burgers vector of the screw dislocation around which the polytype is initially grown. This mis-stacking of the crystallographic planes propagates periodically into every other few planes (depending on the value of the Burgers vector) around the screw dislocation and finally transforms the crystal to another polytype with a different type of stacking of close-packed planes. This is known as the "periodic slip process".[31−33] Based on the fact that the initial hexagonal sheets were grown by the same screw dislocation-driven mechanism and our observation that the phase-transformation occurred around the dislocation, it is reasonable to make an analog of the periodic slip process to the phase transformation in the ZHDS sheets, as shown in Figure 3c: the zinc vacancies started on the surface hexagonal zinc hydroxide layers (due to limited zinc supply, *vide infra*), and then the frontier of the orthorhombic-ordered zinc vacancies slipped periodically further into the crystals along the spiral growth paths of the hexagonal ZHDS sheets, and finally transformed the hexagonal ZHDS sheets to orthorhombic ZHDS sheets completely.

There is yet another resemblance that the ZHDS sheets bear to the polymorphism of ZnS and SiC as well as other crystals. That is, the growth of ZHDS sheets follows the Ostwald's rule of stages, which says that crystallization from solutions often starts with thermodynamically unstable phases followed by a transformation to thermodynamically stable phases.[34−37] We conducted experiments with different starting concentrations of precursors and observed the onset time of the phase transformation to investigate the driving forces of the phase transformation. Figure 4 plots the concentration of $Zn^{2+}$ and $DS^-$ ions *versus* reaction time. Three experiments were done in parallel and the starting concentrations of $Zn^{2+}$ and $DS^-$ ions were 25 and 30 mM (Exp. 1), 25 and 20 mM (Exp. 2), and 10 and 20 mM (Exp. 3), respectively. The time at which the phase transformation started in the above three experiments was 13, 16, and 17 h, respectively. First, we see that higher concentration of SDS curtailed the time it needed to initiate the phase transformation significantly (Exp. 1 and Exp. 2) while a higher concentration of zinc precursor only promoted the phase

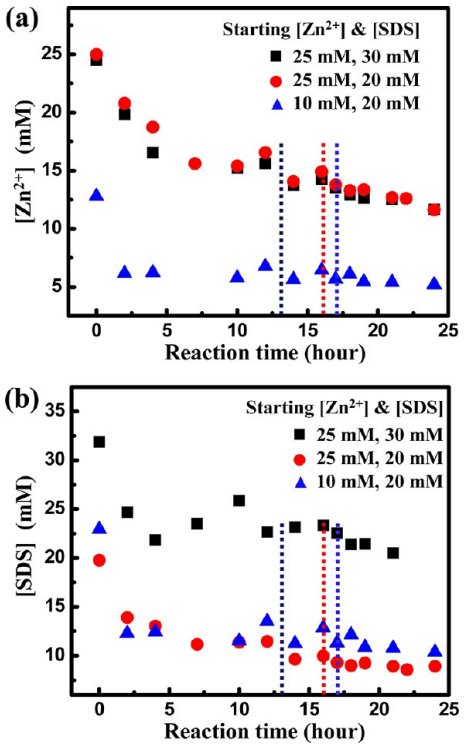


**Figure 4. Investigation of reactants concentration effects. (a) $Zn^{2+}$ and (b) SDS concentration profiles *versus* growth time in three parallel experiments where the starting concentrations of $Zn^{2+}$ and SDS were 25 and 30 mM (Exp. 1), 25 and 20 mM (Exp. 2), and 10 and 20 mM (Exp. 3), respectively. The black, red, and blue dashed lines mark the time when the phase transformation initiated in Exp. 1, 2, and 3, respectively.**

transformation marginally (Exp. 2 and Exp. 3). Therefore, $DS^-$ ions are a vital driver to the phase transformation. This makes more sense when we consider the fact that there is a great content of $DS^-$ with respect to $Zn^{2+}$ in the rectangular ZHDS sheets than in the hexagonal ZHDS sheets due to zinc vacancies. The rectangular ZHDS sheets with higher stoichiometric $DS^-$ would be more stable in a $DS^-$-sufficient environment, especially on the water surface with a close-packed $DS^-$ monolayer. Second, we see that the concentrations of $Zn^{2+}$ and $DS^-$ ions reached a stable regime in less than 10 h while the phase transformation occurred much later than entering this regime. In fact, the concentrations of $Zn^{2+}$ and $DS^-$ ions remained fairly high after extended reaction time. This implied that it was not the exhaustion of the precursors that induced the phase transformation. The phase transformation occurred when the solution was still supersaturated. For example, the phase-transformation in Exp. 1 (black square dots in Figure 4) occurred at 13 h, when the concentrations of both $Zn^{2+}$ and $DS^-$ ions were even higher than those in Exp. 3 (blue triangular dots in Figure 4) at 2 h at which point the hexagonal sheets were still growing.

Based on the observations, we believe that it is the precursor diffusion rather than the bulk precursor

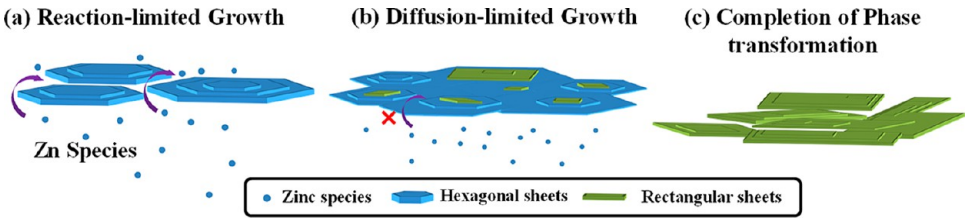


**Figure 5. Schematic illustration of the phase transformation mechanism due to $Zn^{2+}$'s capability of diffusing to growth sites of ZHDS sheets on water surface. (a) Reaction-limited growth stage: at the beginning of sheet growth, the $Zn^{2+}$ diffusion was free and sufficient for ZHDS hexagonal plates. (b) Diffusion-limited growth stage: after a continuous and thick ZHDS was formed, diffusion of $Zn^{2+}$ became difficult and thus deficient for ZHDS growth. The phase transformation was thus triggered. (c) More stable rectangular ZHDS sheets were completely formed by consumption of hexagonal ZHDS sheets.**

concentration that limited the supply of Zn precursors and triggered the phase transformation, as illustrated in Figure 5. In the early stages of the growth (before 4 h), the hexagonal sheets on the water surface were either discrete or joint together by thin surfactant layers. Under this situation, Zn precursors can diffuse freely to the growth sites (*i.e.*, the screw dislocation step edges) near the water surface and the hexagonal sheet growth is at its maximum rate. This is the stage of *reaction-limited growth* (Figure 5a). After ~4 h, there formed a continuous ZHDS nanomembrane covering the entire water surface as we reported previously. As this large-area, continuous ZHDS membrane grew thicker, it became more and more difficult for the $Zn^{2+}$ ions to diffuse to the water surface and reach the growth sites. The growth then entered to the *diffusion-limited stage* (Figure 5b), although the precursors in the bulk solution were still sufficient. Lack of $Zn^{2+}$ triggered the formation of the zinc vacancies, followed by the periodic slip process as discussed earlier that completed the phase transformation (Figure 5c). Combining the two above-mentioned arguments, we conclude that a surplus of $DS^-$ ions and a deficient diffusion of $Zn^{2+}$ ions have collectively driven the phase transformation to the thermodynamically more stable rectangular ZHDS sheets.

**Mechanical Properties of ZHDS Nanomembranes.** Mechanical properties of ZHDS nanomembranes were investigated using nanoindentation. For comparison, nanoindentation was also performed on ZnO single-crystal sheets synthesized by chemical vapor deposition. The load-depth trace of a representative ZnO single crystal sheet indent is shown in Figure 6a and is typical for a single crystal ceramic material. At low loads elastic behavior is observed with loading and unloading segments tracing back and forth on top of each other. Incipient plasticity, indicated by the "pop-in", is the beginning of the elastic-plastic regime. The load-depth trace of a typical ZHDS nanomembrane indent (Figure 6b) exhibits much different behavior. Unloading–loading hystereses show the ZHDS nanomembrane has viscoelasticity. Sudden jumps in depth (indicated by vertical red arrows in Figure 6b) are indicative of inhomogeneous deformation events. Insights into the potential sources for these inhomogeneous deformation events

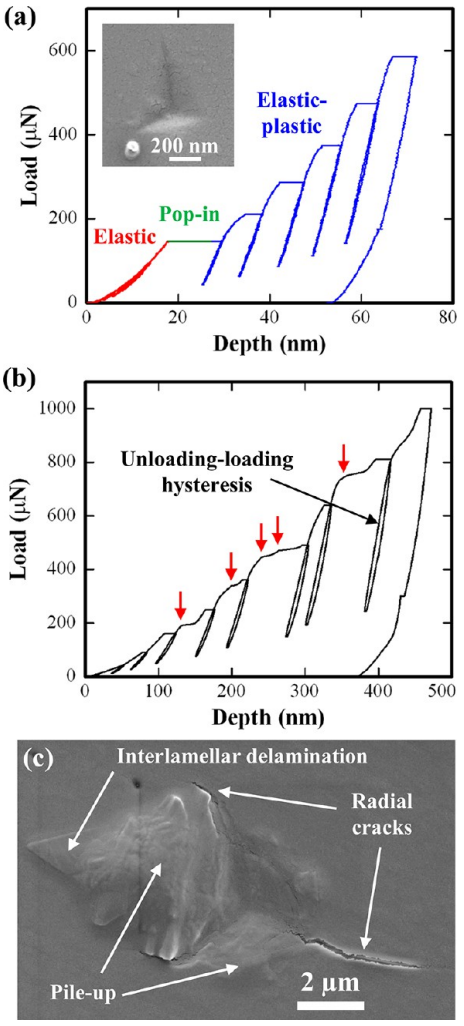


**Figure 6. Mechanical property investigation with nanoindentation. (a) Load-depth trace of multiload indent on a 432 nm ZnO single crystal sheet on a silicon substrate. Inset is an SEM image of the residual indent impression. (b) Load-depth trace of multiload indent on a 954 nm ZHDS nanomembrane on a silicon substrate. Red arrows indicate inhomogeneous deformation events. (c) SEM image of the ZHDS nanomembrane residual indent impression showing the potential sources of the inhomogenous deformation events observed in the ZHDS nanomembrane load-depth trace.**

are observed in the residual indent image (Figure 6c) and include formation of radial cracks extending from the vertices of the residual indent impression and material pile-up at the edges. The sharp features in

the pile-up suggest that intralamellar fracture and interlamellar delamination in the organic layer are mechanisms that contribute to the pile-up. In contrast, the ZnO nanosheet residual indent (inset of Figure 6a) looks relatively featureless. Finally, the ZHDS nanomembrane is much softer than the ZnO nanosheet. Using the standard Oliver-Pharr analysis[38] on the final unloading segment, a 3.2 GPa hardness is estimated for the ZnO nanosheet, which is within the range of previous Berkovich nanoindentation of bulk ZnO single crystals.[39] ZHDS nanomembranes are much softer with a 0.2 GPa hardness, more typical of a structural polymer such as polycarbonate.[40]

**Exfoliation and Dehydration of ZHDS Sheets to ZnO Nanosheets.** Removing the dodecylsulfate ions from the ZHDS sheets and preparing ZnO nanosheets is necessary to fulfill the full potential of this 2-D nanostructure. Exfoliation of layered crystals is common in producing 2-D nanosheets.[41−43] The predominant mechanism of exfoliation is to break the weak interlayer interactions (hydrogen bond, Van de Waals force, *etc.*). Sometimes an ions-exchange reaction is needed to space out the layers before the exfoliation.[44,45] Exfoliation of zinc hydroxide salts has attracted much attention but most reports appear to be either unsuccessful or unconvincing in whether zinc hydroxide is converted to ZnO.[46−48] In addition to zinc hydroxide-to-ZnO conversion (referred to as dehydration in below), another obstacle lies in the fact that layered zinc hydroxy salts are not strictly layered crystals with weak binding forces as in our case where the zinc hydroxide layers are thought to be connected along the spiral growth path. They are just regular crystals with an extremely large lattice parameter along *c*-axis. Up to date, screening the exfoliation solvents remains experiential and detailed exfoliation and dehydration mechanism is generally overlooked.

We focused on the anionic nature of dodecylsulfate ions and took the advantage of electrostatic force. We adopted a method using *n*-butylamine for converting zinc/copper hydroxy chloride powder to ZnO/CuO powder.[49] By transferring the rectangular ZHDS sheets to *n*-butylamine, we successfully removed the dodecylsulfate ions and converted the zinc hydroxide layers to ZnO nanosheets. The ZnO phase was first confirmed by powder X-ray diffraction pattern of the precipitates resulted from the exfoliation (Figure S2). Figure 7 shows TEM images of the exfoliated ZnO nanosheets. At low magnification (Figure 7a), ribbon-like ZnO nanosheets were ubiquitous and most of them were rolled up due to the surface strains coupled with their ultrathin nature. The high-resolution TEM image in Figure 7b shows the polycrystalline nature of the ZnO nanosheets, which echoes the polycrystalline diffraction pattern in the inset of Figure 7a. The single-crystalline grain size in some of the ZnO nanosheets was as large as a few hundred nanometers as is shown

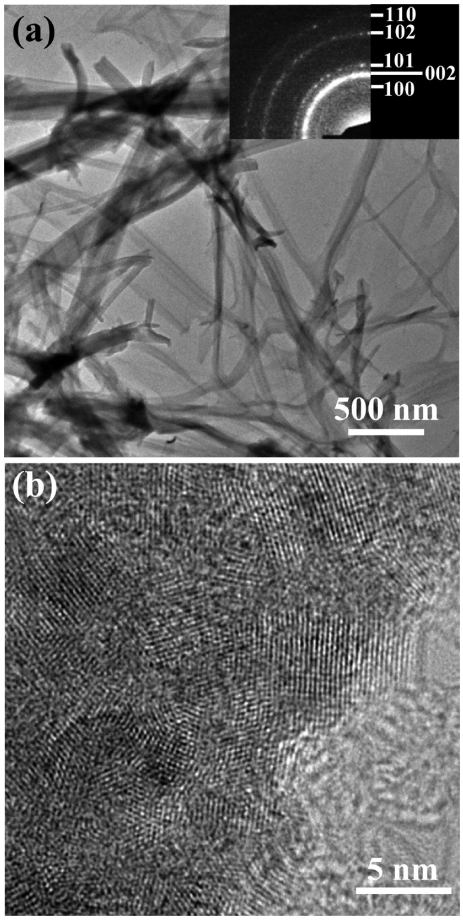


**Figure 7. Exfoliation of ZHDS nanosheets. (a) Low-magnification TEM images of the mostly rolled-up ZnO nanosheets after exfoliation. The inset shows the electron diffraction pattern of the ZnO nanosheets in view. (b) High-resolution TEM image of an unrolled ZnO nanosheet with a polycrystalline nature.**

by SEM and TEM images in the Supporting Information (Figure S3). The converted ZnO nanosheets were as thin as 4 nm, which is shown in Figure S4. We think the polycrystallinity resulted from the chemical reaction-induced strain during the exfoliation process, in which *n*-butylamine acted as both the exfoliating reagent and the dehydration reagent. The reaction could be written as

$$Zn(OH)_2 \cdot Zn(DS)_2 + 2C_4H_{11}N \rightarrow 2ZnO + 2C_4H_{11}NH^+ \cdot DS^-$$

While a dedicated mechanistic study of this reaction is beyond the scope of this work, we could still make some inferences on the reaction process given the crystal structure of ZHDS and the chemical properties of organic amines. In the zinc hydroxide layer of the ZHDS, the zinc cations are highly polarizing, and the O−H groups are directed perpendicular to the layer and are strongly polarized.[50] The protons on the O−H groups thus have a propensity for forming hydrogen bonds with oxygen on the sulfate groups and interlayer water molecules, as well as nitrogen on the *n*-butylamine. They are therefore subject to leave. There are two possible paths for the proton to leave. It could

bond with a DS ion and form dodecylsulfuric acid that subsequently combines with *n*-butylamine *via* an acid−base reaction. Or it could bond directly with *n*-butylamine and form a cationic surfactant that subsequently combines with a $DS^-$ ion. In both cases, organic salts *n*-butylammonium dodecylsulfate ($C_4H_{11}NH^+ \cdot DS^-$) are formed as byproducts of the dehydration and exfoliation process.

## CONCLUSIONS

In this paper, we report a follow-up discovery on the surfactant-directed synthesis of large-area free-standing ZHDS nanomembranes. A spontaneous phase transformation from the hexagonal ZHDS sheets to rectangular ZHDS sheets was observed during extended growth time. We studied the crystal structure of the rectangular ZHDS sheets and concluded a zinc vacancy superlattice in the zinc hydroxide layers. The zinc vacancies could be fitted into an orthorhombic crystal system and have resulted in the formation of the rectangular morphology. The phase transformation started with a metastable ZHDS to a thermodynamically more stable phase and was driven by the $DS^-$-sufficient environment and the limited diffusion of $Zn^{2+}$ ions. The phase transformation was triggered by zinc vacancies which subsequently developed along the spiral growth trajectory around the screw dislocation. The occurrence and process of this phase transformation echoed the canonical Ostwald's rule of stages and periodic slip process, respectively. These investigations gave us a further understanding of the growth and stability of ZHDS nanomembranes as well as other layered metal hydroxide salts. We also demonstrated an effective one-step method for converting ZHDS to ZnO nanosheets, which paved the way for the realization of their potential applications. The ZnO nanosheets only can be obtained from the rectangular ZHDS nanomembranes due to their superior stability, which underscores one aspect of the significance of the new rectangular phase. We also demonstrated the hardness of ZHDS nanomembranes is similar to structural polymers, which represents a radical change in mechanical behavior from ZnO single crystals after the incorporation of surfactant molecules. The use of organic amines for dehydrating metal hydroxide and removing intercalated anionic surfactants added a new tool for the exfoliation of inorganic layered compounds. This research can provide advisory insights on the further development of solution synthesis of free-standing 2-D nanostructures. Further development of this novel nanomembrane self-assembly technique includes controlling the nanomembrane's thickness, increasing the size of their single-crystal grains and the overall crystallinity, as well as studying atomic-scale physical properties, which will pave the road toward a new family of 2D nanomaterial building blocks for flexible, stretchable and transparent electronic devices.

## METHOD

The growth procedures of the initial nanomembranes that comprised of hexagonal crystal grains were reported previously.[20] In brief, we added an excess amount of sodium dodecylsulfate (SDS) (typically 20 mM) in a solution containing a typical amount of 25 mM zinc nitrate and hexamethylenetetramine (HMT). We observed a continuous free-standing membrane that covered the entire opening area of the reaction container at the water surface after about four hours. By further sitting the reaction container under the growth condition, the hexagonal-to-rectangular phase transformation was found starting in about 16 h. The phase transformation completed and rectangular sheets were obtained in about 20 h of reaction. We scooped the membrane from the water surface using different substrates for various further characterizations. To capture the evolution of the phase transformation, ZHDS membranes at the water surface were transferred out at different growth time to silicon substrates or lacey-carbon TEM grids for scanning electron microscope (SEM) and transmission electron microscope (TEM) characterization, respectively.

The morphology and structural characterizations were performed with LEO 1530 SEM and Philips CM200UT TEM. The topography of the ZHDS sheets was scanned by atomic force microscopy (AFM, Park Systems, XE-70) in tapping mode. Small-angle XRD was taken by Hi-Star 2-D X-ray diffractometer and powder diffraction was taken by STOE powder diffractometer. X-ray photoelectron spectroscopy was performed by Thermal Scientific K-Alpha small spot photoelectron spectrometer system. The concentrations of $Zn^{2+}$ and dodecylsulfate ($DS^-$) ions in the growth solution at different reaction time were determined by inductively coupled plasma atomic emission spectroscopy (ICP-AES). The growth solution were sampled at different time during the reaction, and subsequently centrifuged to remove solid precipitates and diluted to a constant volume. Zinc sulfate was used to prepare the standard solutions for the working curve. The interface adsorption of $DS^-$ ions in the tubing of the ICP-AES system made it difficult to quantify the concentration of sulfur. To solve this problem, perchloric acid was added to sever the sulfate group from the hydrocarbon chain and therefore all sulfur was in the form of free sulfate groups. A Hysitron (Minneapolis, MN) TriboIndenter equipped with a Berkovich probe was used to investigate the mechanical properties of ZHDS nanomembranes.

Exfoliation of rectangular ZHDS sheets was done by transferring the as-grown sheets to *n*-butylamine solution. This solution was kept sitting for two days and then drop-cast to a TEM grid for imaging. The exfoliated ZnO nanosheets were collected for powder X-ray diffraction by adding acetone to *n*-butylamine to let the ZnO nanosheets precipitate.

*Conflict of Interest:* The authors declare no competing financial interest.

*Acknowledgment.* We thank Dr. Jian Shi for his help on TEM characterization. This research is supported by UW-NSF Nanoscale Science and Engineering Center (NSEC) (DMR 0425880), DARPA N66001-11-1-4139, and NSF CAREER CMMI-1148919.

*Supporting Information Available:* This section includes the X-ray photoelectron spectra of hexagonal and rectangular ZHDS sheets, X-ray powder diffraction pattern of exfoliated ZnO nanosheets, TEM images of exfoliated ZnO nanosheets with large single-crystalline dimensions, and an AFM

topography image of a 4 nm thin ZnO nanosheet. This material is available free of charge *via* the Internet at http://pubs.acs.org.

## REFERENCES AND NOTES


1. Geim, A. K. Graphene: Status and Prospects. *Science* **2009**, *324*, 1530–1534.
2. Rao, C. N. R.; Sood, A. K.; Subrahmanyam, K. S.; Govindaraj, A. Graphene: The New Two-Dimensional Nanomaterial. *Angew. Chem., Int. Ed.* **2009**, *48*, 7752–7777.
3. Rogers, J. A.; Lagally, M. G.; Nuzzo, R. G. Synthesis, Assembly and Applications of Semiconductor Nanomembranes. *Nature* **2011**, *477*, 45–53.
4. Allen, M. J.; Tung, V. C.; Kaner, R. B. Honeycomb Carbon: A Review of Graphene. *Chem. Rev.* **2010**, *110*, 132–145.
5. Huang, M. H.; Cavallo, F.; Liu, F.; Lagally, M. G. Nanomechanical Architecture of Semiconductor Nanomembranes. *Nanoscale* **2011**, *3*, 96–120.
6. Eda, G.; Fanchini, G.; Chhowalla, M. Large-Area Ultrathin Films of Reduced Graphene Oxide as a Transparent and Flexible Electronic Material. *Nat. Nanotechnol.* **2008**, *3*, 270–274.
7. Monch, I.; Schumann, J.; Stockmann, M.; Arndt, K. F.; Schmidt, O. G. Multifunctional Nanomembranes Self-Assembled into Compact Rolled-Up Sensor-Actuator Devices. *Smart Mater. Struct.* **2011**, 20.
8. Park, S. I.; Xiong, Y. J.; Kim, R. H.; Elvikis, P.; Meitl, M.; Kim, D. H.; Wu, J.; Yoon, J.; Yu, C. J.; Liu, Z. J.; *et al.* Printed Assemblies of Inorganic Light-Emitting Diodes for Deformable and Semitransparent Displays. *Science* **2009**, *325*, 977–981.
9. Zhou, H.; Seo, J. H.; Paskiewicz, D. M.; Zhu, Y.; Celler, G. K.; Voyles, P. M.; Zhou, W. D.; Lagally, M. G.; Ma, Z. Q. Fast Flexible Electronics with Strained Silicon Nanomembranes. *Sci. Rep.* **2013**, 3.
10. Choi, H.-J.; Jung, S.-M.; Seo, J.-M.; Chang, D. W.; Dai, L.; Baek, J.-B. Graphene for Energy Conversion and Storage in Fuel Cells and Supercapacitors. *Nano Energy* **2012**, *1*, 534–551.
11. Nikoobakht, B.; Li, X. L. Two-Dimensional Nanomembranes: Can They Outperform Lower Dimensional Nanocrystals? *ACS Nano* **2012**, *6*, 1883–1887.
12. Viventi, J.; Kim, D. H.; Moss, J. D.; Kim, Y. S.; Blanco, J. A.; Annetta, N.; Hicks, A.; Xiao, J. L.; Huang, Y. G.; Callans, D. J.; *et al.* A Conformal, Bio-Interfaced Class of Silicon Electronics for Mapping Cardiac Electrophysiology. *Sci. Transl. Med.* **2010**, 2.
13. Kaniyoor, A.; Ramaprabhu, S. An Optically Transparent Cathode for Dye Sensitized Solar Cells Based on Cationically Functionalized and Metal Decorated Graphene. *Nano Energy* **2012**, *1*, 757–763.
14. Kim, S.; Wu, J. A.; Carlson, A.; Jin, S. H.; Kovalsky, A.; Glass, P.; Liu, Z. J.; Ahmed, N.; Elgan, S. L.; Chen, W. Q.; Ferreira, P. M.; *et al.* Microstructured Elastomeric Surfaces with Reversible Adhesion and Examples of Their Use in Deterministic Assembly by Transfer Printing. *Proc. Natl. Acad. Sci. U.S.A.* **2010**, *107*, 17095–17100.
15. Ko, H. C.; Baca, A. J.; Rogers, J. A. Bulk Quantities of Single-Crystal Silicon Micro-/Nanoribbons Generated from Bulk Wafers. *Nano Lett.* **2006**, *6*, 2318–2324.
16. Yoon, J.; Jo, S.; Chun, I. S.; Jung, I.; Kim, H. S.; Meitl, M.; Menard, E.; Li, X. L.; Coleman, J. J.; Paik, U.; *et al.* GaAs Photovoltaics and Optoelectronics Using Releasable Multilayer Epitaxial Assemblies. *Nature* **2010**, *465*, 329–330.
17. Schliehe, C.; Juarez, B. H.; Pelletier, M.; Jander, S.; Greshnykh, D.; Nagel, M.; Meyer, A.; Foerster, S.; Kornowski, A.; Klinke, C.; *et al.* Ultrathin PbS Sheets by Two-Dimensional Oriented Attachment. *Science* **2010**, *329*, 550–553.
18. Yu, T.; Lim, B.; Xia, Y. N. Aqueous-Phase Synthesis of Single-Crystal Ceria Nanosheets. *Angew. Chem., Int. Ed.* **2010**, *49*, 4484–4487.
19. Yang, X. H.; Li, Z.; Liu, G.; Xing, J.; Sun, C.; Yang, H. G.; Li, C. Ultra-Thin Anatase $TiO_2$ Nanosheets Dominated with {001} Facets: Thickness-Controlled Synthesis, Growth Mechanism and Water-Splitting Properties. *CrystEngComm* **2011**, *13*, 1378.
20. Wang, F.; Seo, J. H.; Ma, Z. Q.; Wang, X. D. Substrate-Free Self-Assembly Approach toward Large-Area Nanomembranes. *ACS Nano* **2012**, *6*, 2602–2609.
21. Danger, B. R.; Fan, D.; Vivek, J. P.; Burgess, I. J. Electrochemical Studies of Capping Agent Adsorption Provide Insight into the Formation of Anisotropic Gold Nanocrystals. *ACS Nano* **2012**, *6*, 11018–11026.
22. Mdluli, P. S.; Sosibo, N. M.; Mashazi, P. N.; Nyokong, T.; Tshikhudo, R. T.; Skepu, A.; van der Lingen, E. Selective Adsorption of PVP on The Surface of Silver Nanoparticles: A Molecular Dynamics Study. *J. Mol. Struct.* **2011**, *1004*, 131–137.
23. Tunik, L.; Addadi, L.; Garti, N.; FurediMilhofer, H. Morphological and Phase Changes in Calcium Oxalate Crystals Grown in the Presence of Sodium Diisooctyl Sulfosuccinate. *J. Cryst. Growth* **1996**, *167*, 748–755.
24. Bakshi, M. S.; Thakur, P.; Sachar, S.; Kaur, G.; Banipal, T. S.; Possmayer, F.; Petersen, N. O. Aqueous Phase Surfactant Selective Shape Controlled Synthesis of Lead Sulfide Nanocrystals. *J. Phys. Chem. C* **2007**, *111*, 18087–18098.
25. Yi, K. C.; Horvolgyi, Z.; Fendler, J. H. Chemical Formation of Silver Particulate Films under Monolayers. *J. Phys .Chem.* **1994**, *98*, 3872–3881.
26. Yang, J. P.; Meldrum, F. C.; Fendler, J. H. Epitaxial-Growth of Size-Quantized Cadmium-Sulfide Crystals under Arachidic Acid Monolayers. *J. Phys. Chem.* **1995**, *99*, 5500–5504.
27. Yang, J. P.; Fendler, J. H. Morphology Control of Pbs Nanocrystallites, Epitaxially under Mixed Monolayers. *J. Phys. Chem.* **1995**, *99*, 5505–5511.
28. Morin, S. A.; Forticaux, A.; Bierman, M. J.; Jin, S. Screw Dislocation-Driven Growth of Two-Dimensional Nanoplates. *Nano Lett.* **2011**, *11*, 4449–4455.
29. Frank, F. C. The Growth Of Carborundum: Dislocations and Polytypism. *Philos. Mag.* **1951**, *42*, 1014–1021.
30. Ding, Y.; Yang, R.; Wang, Z. L. Ordered Zinc-Vacancy Induced $Zn_{0.75}O_x$ Nanophase Structure. *Solid State Commun.* **2006**, *138*, 390–394.
31. Alexande., E.; Kalman, Z. H.; Mardix, S.; Steinber, It Mechanism of Polytype Formation in Vapour-Phase Grown Zns Crystals. *Philos. Mag.* **1970**, *21*, 1237–1246.
32. Powell, J. A.; Will, H. A. Low-Temperature Solid-State Phase-Transformation in 2h Silicon-Carbide. *J. Appl. Phys.* **1972**, *43*, 1400–1408.
33. Mardix, S.; Kalman, Z. H.; Steinber, I. T. Periodic Slip Processes and Formation of Polytypes in Zinc Sulphide Crystals. *Acta Crystallogr.* **1968**, *A 24*, 464–469.
34. Stoica, C.; Verwer, P.; Meekes, H.; Vlieg, E.; van Hoof, P. J. C. M.; Kaspersen, F. M. Epitaxial 2D Nucleation of the Stable Polymorphic Form of the Steroid 7 Alpha MNa on the Metastable Form: Implications for Ostwald's Rule of Stages. *Int. J. Pharm.* **2006**, *309*, 16–24.
35. Schmelzer, J.; Moller, J.; Gutzow, I. Ostwald's Rule of Stages: the Effect of Elastic Strains and External Pressure. *Z. Phys. Chem.* **1998**, *204*, 171–181.
36. Nyvlt, J. The Ostwald Rule of Stages. *Cryst. Res. Technol.* **1995**, *30*, 443–449.
37. Feenstra, T. P.; Debruyn, P. L. The Ostwald Rule of Stages in Precipitation from Highly Supersaturated Solutions—a Model and Its Application to the Formation of the Non-stoichiometric Amorphous Calcium-Phosphate Precursor Phase. *J. Colloid Interface Sci.* **1981**, *84*, 66–72.
38. Oliver, W. C.; Pharr, G. M. An Improved Technique for Determining Hardness and Elastic-Modulus Using Load and Displacement Sensing Indentation Experiments. *J. Mater. Res.* **1992**, *7*, 1564–1583.
39. Lucca, D. A.; Klopfstein, M. J.; Ghisleni, R.; Cantwell, G. Investigation of Polished Single Crystal ZnO by Nanoindentation. *CIRP Ann.* **2002**, *51*, 483–486.
40. Jakes, J. E.; Lakes, R. S.; Stone, D. S. Broadband Nanoindentation of Glassy Polymers: Part II. Viscoplasticity. *J. Mater. Res.* **2012**, *27*, 475–484.
41. Hernandez, Y.; Nicolosi, V.; Lotya, M.; Blighe, F. M.; Sun, Z. Y.; De, S.; McGovern, I. T.; Holland, B.; Byrne, M.; Gun'ko, Y. K.; *et al.* High-Yield Production of Graphene by Liquid-Phase

Exfoliation of Graphite. *Nat. Nanotechnol.* **2008**, *3*, 563–568.
42. Coleman, J. N.; Lotya, M.; O'Neill, A.; Bergin, S. D.; King, P. J.; Khan, U.; Young, K.; Gaucher, A.; De, S.; Smith, R. J.; *et al.* Two-Dimensional Nanosheets Produced by Liquid Exfoliation of Layered Materials. *Science* **2011**, *331*, 568–571.
43. Liu, J.; Poh, C. K.; Zhan, D.; Lai, L.; Lim, S. H.; Wang, L.; Liu, X.; Gopal Sahoo, N.; Li, C.; Shen, Z.; Lin, J. Improved Synthesis of Graphene Flakes from the Multiple Electrochemical Exfoliation of Graphite Rod. *Nano Energy* **2013**, *2*, 377–386.
44. Fu, X.; Qutubuddin, S. Polymer-Clay Nanocomposites: Exfoliation of Organophilic Montmorillonite Nanolayers in Polystyrene. *Polymer* **2001**, *42*, 807–813.
45. Omomo, Y.; Sasaki, T.; Wang, L. Z.; Watanabe, M. Redoxable Nanosheet Crystallites of $MnO_2$ Derived *via* Delamination of A Layered Manganese Oxide. *J. Am. Chem. Soc.* **2003**, *125*, 3568–3575.
46. Altuntasoglu, O.; Matsuda, Y.; Ida, S.; Matsumoto, Y. Syntheses of Zinc Oxide and Zinc Hydroxide Single Nanosheets. *Chem. Mater.* **2010**, *22*, 3158–3164.
47. Zhang, W. X.; Yanagisawa, K. Hydrothermal Synthesis of Zinc Hydroxide Chloride Sheets and Their Conversion to ZnO. *Chem. Mater.* **2007**, *19*, 2329–2334.
48. Chen, W.; Feng, L.; Qu, B. J. Preparation of Nanocomposites by Exfoliation of ZnAl Layered Double Hydroxides in Nonpolar LLDPE Solution. *Chem. Mater.* **2004**, *16*, 368–370.
49. Garciamartinez, O.; Rojas, R. M.; Vila, E.; Devidales, J. L. M. Microstructural Characterization of Nanocrystals of ZnO and CuO Obtained from Basic Salts. *Solid State Ionics* **1993**, *63−5*, 442–449.
50. Evans, D. G.; Slade, R. C. T. Structural Aspects of Layered Double Hydroxides. *Struct. Bonding (Berlin, Ger.)* **2006**, *119*, 1–87.